A New Proposal to Jefferson Lab PAC-25

Measurement of G_E^p/G_M^p using elastic $\vec{p}(\vec{e},e')p$ up to $Q^2 = 3.50$ (GeV/c)^2

$\star\star\star$ **DRAFT** November 14, 2003$\star\star\star$

X. Zheng[1]
Argonne National Laboratory, Argonne, IL 60439

J.R. Calarco
University of New Hampshire, Durham, NH 03824

Abstract

We propose here measurements G_E^p/G_M^p via doubly polarized elastic $\vec{p}(\vec{e},e')p$ scattering at $Q^2 = 2.10$ and 3.50 (GeV/c)^2. The UVa polarized NH_3 target will be used in Hall C with its spin aligned 139° w.r.t. beam direction. To extract G_E^p/G_M^p, we perform single-arm electron measurements at kinematics where the elastic asymmetries are the most sensitive to this ratio. In addition, the asymmetry will be measured at $Q^2 = 0.19$ (GeV/c)^2 to determine the absolute electron beam helicity state and to check the product of beam and target asymmetries. Assuming 80% beam polarization and 85 nA current, we request 14 days of total beam time to achieve precision of $\Delta(\mu G_E^p/G_M^p) = 0.060$ and 0.071 at $Q^2 = 2.10$ and 3.50 (GeV/c)^2, respectively. We request four days overhead time. The proposed measurement will provide the first data of G_E^p/G_M^p from the $\vec{p}(\vec{e},e')p$ asymmetry method in intermediate Q^2 range to a good precision. The new method is possiblly less sensitive to the two-photon exchange effect than Rosenbluth separation and it has different systematic uncertainties than polarization transfer method, hence will complement these two technique and provide valuable information on the proton form factors.

Contents

[1]Email: xiaochao@jlab.org

1 Motivation

The nucleon is one of the basic building blocks of nature. The elastic form factors are the most important fundamental properties of the nucleon, describing its internal structure due to the spatial distribution of its charge and magnetism. Thus they are the most basic nucleonic properties we can measure. Not only do they play an essential role in hadronic physics as the *sine qua non* input to our understanding of nucleon structure, but they also serve to test the Standard Model. Hence it is of the utmost urgency that we have accurate and reliable measurements of these fundamental characteristics of the nucleon from low Q^2 to the highest Q^2 we can reach. However, there appears to be a discrepancy between values obtained by two very different techniques that clearly indicates a problem in either the experimental methods or the theoretical basis used to extract the form factors from the data. Any such discrepancies must be resolved without delay. In this proposal, we propose an independent measurement of the ratio $\mu G_E/G_M$ on the proton using a third technique which is experimentally unrelated to either of the first two.

1.1 Theories

In this section we briefly review available calculations for G_E^p/G_M^p, then give an overview of previous world data and propose a new method to measure G_E^p/G_M^p.

The proton elastic form factors have been calculated in various models. At $Q^2 < 1$ (GeV/c)^2, the Vector Meson Dominance (VMD) model [1] successfully describes the nucleon form factors. In the high Q^2 region, the dominant degrees of freedom of the nucleon are the three valence quarks and perturbative Quantum Chromo-Dynamics (pQCD) theory can be applied [2]. Specifically, based on the leading-order pQCD, or hadron helicity conservation, the ratio of Dirac and Pauli form factors F_2^p/F_1^p is expected to scale as $1/Q^2$ at high Q^2 [2, 3], which directly constrains the behavior of G_E^p/G_M^p in this region.

In the intermediate region $1 < Q^2 < 20$ (GeV/c)^2, however, predictions for the nucleon form factors become difficult because the soft scattering processes are still dominant compared to hard scattering. Moreover, these soft contributions might be different for different observables

Figure 1: Previous world data for $\mu G_E^p/G_M^p$ compared with various calculations including that from VMD (black) [1], the cloudy bag model [8], RCQM (red curve) [5], PSFA (green) [6], SU(6) breaking with CQM fFF (blue) [7] and chiral soliton model (magenta) [9]. Data below $Q^2 = 1$ (GeV/c)^2 are not shown for clarity.

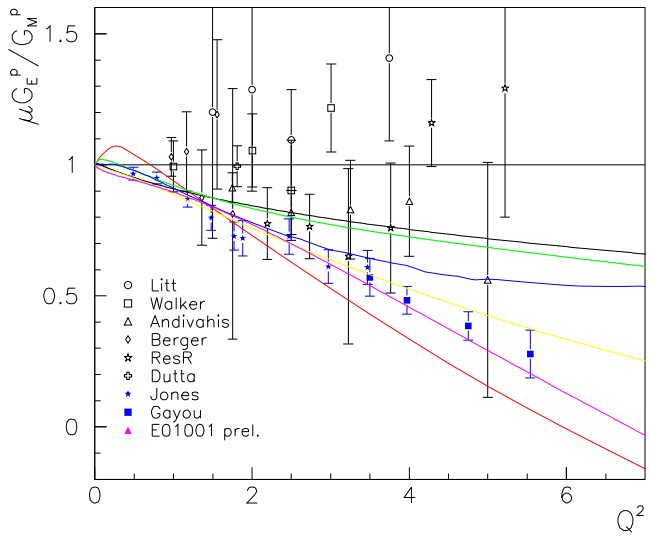

of the scattering processes. This fact itself can be used as a tool to understand the role of the soft processes without reaching asymptotically high Q^2. Many QCD models have been used to calculate the elastic nucleon form factors in this region - the relativistic constituent quark model (RCQM) [4, 5], the cloudy bag model (CBM) [8], the SU(6) breaking CQM [7], the point-form spectator approximation (PFSA) model based on the Goldstone boson exchange CQM [6], and

the chiral soliton model [9]. Figure 1 shows existing calculations for $\mu G_E^p/G_M^p$ along with the world data.

1.2 Existing Data

The proton elastic form factors have been measured for almost five decades. In the traditional Rosenbluth separation method, based on the assumption of the one photon exchange process, the elastic cross section is measured at fixed four momentum transfer Q^2 but different values of photon polarization ϵ. Then the values of G_E^p, G_M^p and their ratio are extracted from a linear fit of the cross section as a function of $1/\epsilon$. This method is usually used at $Q^2 < 9$ (GeV/c)^2. Data from this method show that G_M^p can be approximated by the dipole form $G_D = \mu_P/(1 + Q^2/0.71)^2$ with μ_P the proton magnetic moment, at least up to about $Q^2 = 3 - 4$ (GeV/C)^2. The ratio $\mu^p G_E^p/G_M^p$ is observed by this method to be close to unity, independent of whether G_M^p follows the dipole ansatz or not. Above this Q^2 region, G_M^p is extracted from single cross section measurements assuming $\mu^p G_E^p = G_M^p$. Data on F_1^p at $Q^2 > 10$ (GeV/c)^2 show a $1/Q^4$ scaling behavior which is consistent with pQCD predictions [11].

However, recent data from the method of measuring the polarization transfer [12, 13, 14] showed that $\mu G_E^p/G_M^p$ drops linearly as Q^2 increases and reaches as low as ≈ 0.3 at $Q^2 = 5.6$ (GeV/c)^2, in significant disagreement with the Rosenbluth data (see Fig. 2). This dramatic change has invoked large interest in both theoretical and experimental aspects of the proton form factor. Different fits have been performed separately to data from Rosenbluth method, and data from both Rosenbluth and polarization transfer methods [17]. Previous Rosenbluth data have been re-analyzed [15] but the results are still inconsistent with polarization measurements. At high Q^2, data from cross section measurements have also been re-analyzed using the polarization transfer fit [13] and are found to be self-consistent [15].

Experimentally, preliminary results from the recently accomplished Hall A experiment E01-001 [18] agree well the traditional Rosenbluth data. A new polarization transfer experiment [19] is being planned in Hall C to measure G_E^p/G_M^p via polarization transfer up to $Q^2 = 9.0$ (GeV/c)^2, using instrumentation independent from the Hall A experiments.

1.3 Two-Photon Exchange Correction

In order to explain the discrepancy between the Rosenbluth separation and polarization transfer data, under the assumption that both are correct, significant effort has been put into understanding the radiative corrections and soft processes that can modify the results obtained from the assumption of one-photon exchange. The validity of radiative corrections has been checked, and it has been suggested that the two-photon exchange process may explain part of the discrepancy between the two data sets.

There is at least a two-photon (and higher order) exchange process that is not accounted for in the Rosenbluth formulation of the $e-p$ scattering cross section. This correction can introduce an ϵ-dependence to the cross section and affect the linearity of Rosenbluth plot. Guichon and

Figure 2: Previous world data for $\mu G_E^p/G_M^p$ from Rosenbluth method (open b&w markers) and from polarization transfer (solid b&w markers). For clarity, data below $Q^2 = 1$ (GeV/c)^2 are not shown. Preliminary results from recent Hall A E01-001 (solid magenta triangles) agree well with Rosenbluth data. Curves are from Bosted parameterization (black) [16], a fit to the Hall A polarization transfer results (blue) [13] and global fits to only Rosenbluth data (red) and both data sets (magenta) [17]. A dramatic disagreement is clearly seen between the two data set at $Q^2 > 2$ (GeV/c)^2.

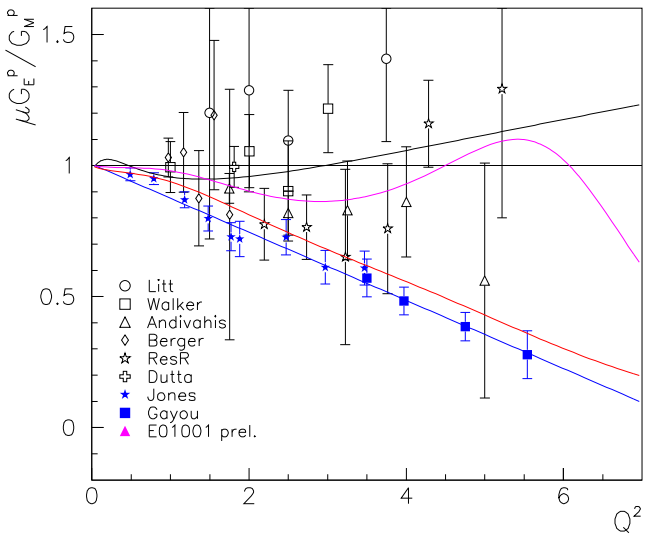

Vanderhaeghen [20] showed that, phenomenologically, the correction to the Rosenbluth data is much larger than to the polarization transfer data, and the true $\mu G_E^p/G_M^p$ is about 20% below the polarization transfer fit. Blunden, Melnitchouk and Tjon [21] evaluated the two-photon exchange contributions to elastic $e-p$ scattering cross sections based on a simple hadronic model including the finite size of the proton. Their results explained one third of the descrepancy between the two data sets. Rekalo and Tomasi-Gustaffson [22] derived from first principles, *i..e.* the C-invariance of the EM interaction and the crossing symmetry, the general properties of two-photon exchange in $e - p$ elastic scattering. They showed again that the presence of this mechanism destroys the linearity of the Rosenbluth separation but does not affect the terms related to the EM form factors.

Basically, there are small (few %) but slightly different corrections to electric and magnetic contributions due to the two photon exchange corrections. In the Rosenbluth separation technique, as Q^2 increases the percentage of the cross section due the G_E decreases to a value of a few % at around 3 (GeV/c)^2 and gets even smaller as Q^2 continues to be increased. Thus an accurate extraction of $\mu G_E/G_M$ as Q^2 increases depends sensitively on accurately knowing the magnetic contribution. A correction of just a few % can produce a large change in the resulting value of $\mu G_E/G_M$, by factors of 2 – 3.

On the other hand, the polarization transfer experiment provides a direct measurement of the ratio $\mu G_E/G_M$. The calculations show that the two-photon contributions to the electric and magnetic components are small to moderate, and in the same direction, but not equal. Therefore, while the ratio $\mu G_E/G_M$ from the spin transfer measurement will be affected by the two-photon exchange contributions, the size of the effect is much less than for the Rosenbluth separation technique and maybe within experimental uncertainties for the higher Q^2 data points.

In this context, it is interesting to note that previous work by Brash *et al.*[**?**] showed that the discrepancy between the ratio $\mu G_E/G_M$ as extracted by the two different techniques, could be resolved by a small change to the magnetic contribution to the $e-p$ cross section. These authors fit the polarization transfer data and then use the results of that fit to reinterpret the Rosenbluth separations. Their results show a slightly larger magnetic form factor than previously inferred. While they offer no physical explanation, this is precisely the direction of the two-photon exchange correction.

The two-photon exchange correction provides an attractive explanation of the discrepancies in the existing data. Furthermore it not only affects the extraction of form factors from $e-p$ scattering, but also affects many other observables, *e.g.* parity-violating asymmetries. A full understanding of this process may take decades. Along this journey, experimental data will provide valuable and necessary guidance to the development of related theories. In fact, there is a direct prediction[ref] that the interference between the one- and two-photon exchange processes leads to a non-zero transverse target polarization asymmetry A_y. An early attempt to measure this at SLAC showed the asymmetry to be zero but within rather large errors [ref]. There has been a recent suggestion to try to measure this asymmetry using BLAST at the MIT-Bates accelerator, and a proposal is also being prepared for Hall C.[**?**] Even if a two-photon effect is measured, there may be other corrections of which we are not aware, that can add to the desprepancy between the two form factor data sets. Therefore we think it is necessary to perform another measurement using a method different from Rosenbluth and polarization transfer.

2 The Proposed Experiment

We propose here a third method to measure G_E^p/G_M^p in the intermediate Q^2 range at $Q^2 = 2.10$ and 3.50 (GeV/c)^2. We will measure the asymmetry of $\vec{e}-\vec{p}$ elastic scattering and the G_E^p/G_M^p ratio will be extracted from measured asymmetries. Formula for doubly polarized elastic scattering and its asymmetries are given in Appendix A. The UVa polarized NH_3 target will be used in Hall C with its spin aligned at 139° w.r.t. beam-line (*i.e.* pointing to the left of the beam-line when viewing toward beam dump). The scattered electrons will be detected in HMS. In addition, the asymmetry at $Q^2 = 0.19$ (GeV/c)^2 will be measured to better than 2% statistical level, which serve to determine the absolute electron helicity state and to check the product of beam and target polarizations.

Assuming 85 nA beam current with 80% polarization, we request 14 days beam time to reach $\Delta(\mu G_E^p/G_M^p) = 0.060$ and 0.071 at $Q^2 = 2.10$ and 3.50 (GeV/c)^2, respectively. The above beam time include nitrogen runs and Møller measurements. Four days overhead time are

needed for beam pass change and target work. The UVa polarized NH_3 target will be installed with un-parallel spin orientation.

The proposed measurement will provide the first data on G_E^p/G_M^p from a third method in the intermediate Q^2 range to a good precision. This method is possiblly less sensitive to the two-photon exchange effect than Rosenbluth separation, also it has different systematic uncertainties compared to polarization transfer technique, hence will complement these two methods. The new results will provide crucial information on both the proton structure and the understanding of previous world data. They will also provide valuable guidance for theoretical work on the two-photon exchange effect.

3 Experimental Setup

In the following we describe the experimental setup for the proposed measurement in Hall C.

3.1 Overview

The floor plan for Hall C is shown in Fig. 4. The UVa polarized NH_3 target will be installed with its spin direction aligned at 139° w.r.t. beam-line. The scattered electrons will be detected by the HMS. Elastic events are identified by the electron scattering angle and momentum and the elastic kinematic conditions.

Figure 3: Hall C floor plan for the proposed measurement (not to scale).

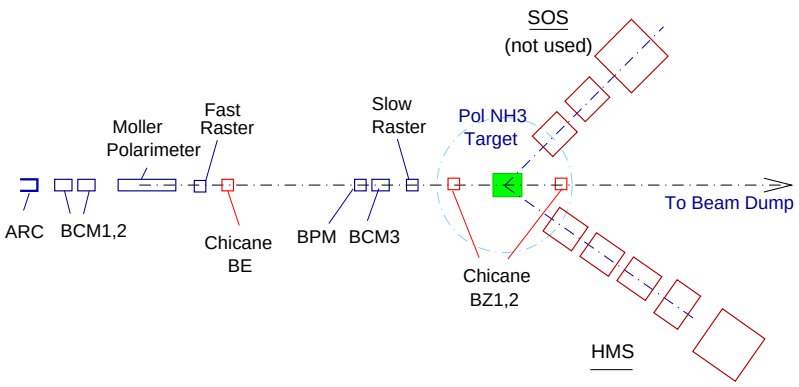

3.2 Beam Line

We propose to use polarized beam with 80% polarization and 85 nA beam current at two beam energies 1.20 and 6.00 GeV. Beam energy will be measured to $\Delta E/E = 2 \times 10^{-4}$ level using ARC method [24]. We plan to use Møller for beam polarization measurement. Currently the

Figure 4: Kinematics for the proposed measurement. Target spin angles are shown for the case when scattering plane is horizontal ($\phi^\star = 0°$). Lightly shaded areas show the blocking of target coils, which cover from $50°$ to $73°$ along either side of the field axis.

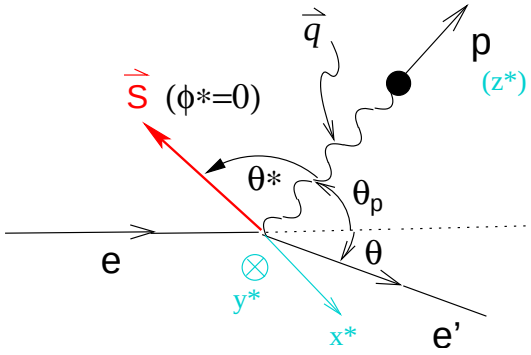

Møller polarimeter in Hall C can provide better than 1% precision. However additional systematic error can come from the fact that we are running at 85 nA low current. We therefore use 1.5% in the uncertainty estimation.

Because the target spin is not parallel to the beam direction, the strong 5 T magnetic field

Figure 5: Hall C beam line chicane magnets and raster system.

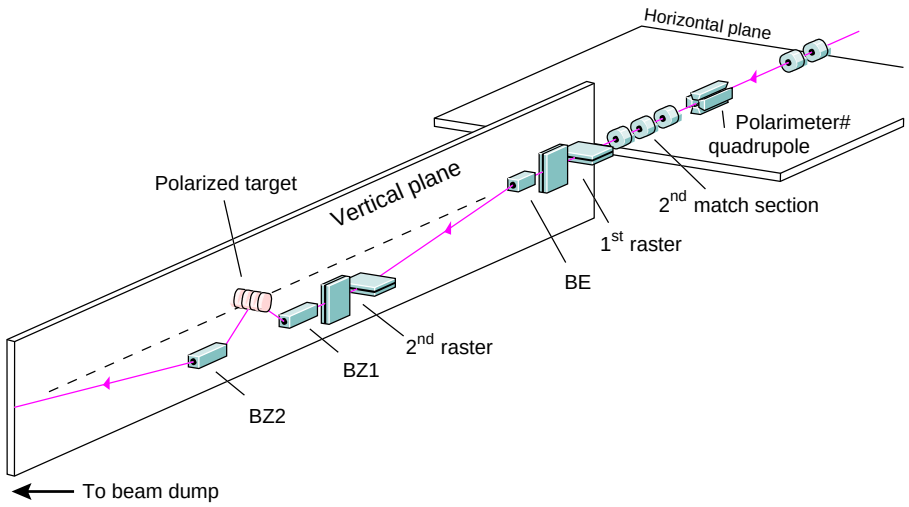

of the target will bend the electron beam toward the floor. In order to ensure that the incoming beam is incident on the target cell horizontally, we will use a chicane magnet to bend the beam

up before it enters the target scattering chamber. In addition, the beam will be bend again after it exits the target such that it will arrive in the beam dump. A series of chicane magnets were used for similar purpose during the G_E^n experiment E93-026 [26, 27] and we will use the same setup.

The beam needs to be rastered to maintain the target polarization and to ensure uniform distribution of both heat and radiation on the target material. We require the beam spot at the target to be ≈ 2 cm in diameter which almost cover the entire target. This has been achieved using the slow rastering system during previous experiments [26, 27]. A schematic diagram for the beam-line chicane magnets and raster system is shown in Fig. 5.

Beam position monitoring and beam current measurement at our low current of 85 nA need special care. Using the same method as previous experiment E93-026, we believe a precise beam position monitoring can be achieved and the beam current can be measured to 5% level. The effect on the measured asymmetry should be negligible.

3.3 The UVa NH_3 Target

We will use a solid polarized proton target developed by the University of Virginia. In this target, Dynamic Nuclear Polarization (DNP) is utilized to enhance the low temperature (≈ 1 K), high magnetic field (5 T) polarization of solid materials. The irradiation of the target with 140 GHz microwaves drives hyperfine transitions hence align the nucleon spins. This target was successfully used in the SLAC experiments E143, E155, E155x and two experiments E93-026 [26] and E01-006 [27] at Hall C. The proton polarization in $^{15}NH_3$ can reach as high as 95% and will decrease because of the beam depolarization effect. An average polarization of 75% was routinely achieved during previous experiments.

The target consists of a superconducting dipole magnet which operates at 5 Tesla, a ^{4}He evaporation refrigerator, a large pumping system, a high power microwave tube operating at frequencies around 140 GHz and a NMR system for measuring the target polarization. Figure 6 shows the target side view.

For the proposed measurement, the target material is $^{15}NH_3$ and the target spin needs to be aligned at 139° w.r.t. beamline. Figure 7 shows the orientation of the target field and coils. For safety reason, 5 mm clearance is required between the raster outer edge and the coil. The target polarization needed is 75% (average) with 85 nA beam, measured by NMR to 2.5% level. The target cell is a 3 cm long cylinder with 1 inch diameter. Figure 8 shows the geometry of the cell and the NMR coil used to measure proton polarization.

The target cell is filled by frozen ammonia granules and is placed into a target holder and lowered into a cryostat of liquid ^{4}He. The nitrogen, helium and other target holder materials are in the acceptance of the spectrometers and will serve to dilute the measured asymmetry. Thickness and density of each material are given in Table 1. Dilution factor will be given in Section 4.4. Moreover, the unpaired proton in nitrogen can be polarized, hence a correction to the asymmetry must be made during analysis. The uncertainty due to nitrogen asymmetry will be given in Section 4.5.

The strong magnetic field at this configuration will have an effect on the scattering charged particles but this can be well simulated and corrected.

The uncertainty in the target spin direction is one of the main systematic uncertainties of this

Figure 6: Sideview of the UVa polarized NH_3 target.

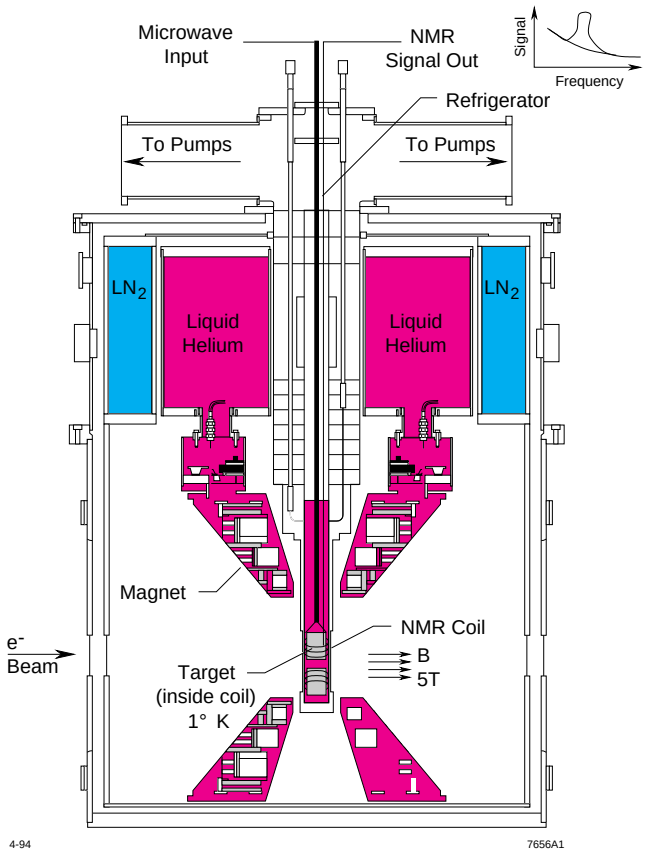

Table 1: Thickness and density for unpolarized materials in acceptance.

Material	Thickness (cm)	Density (g/cm^3)
^{4}He	0.37	0.145
Al end-caps	0.00762	2.70
Copper in NMR coil	0.00673	8.96
Nickel in NMR coil	0.00289	8.75
Titanium windows in tail	0.00712	4.54
Al windows in LN_2 shield	0.00508	2.70
Al entrance window in cryostat	0.00702	2.70
Al exit window in cryostat	0.01016	2.70

Figure 7: Cofiguration of target coils.

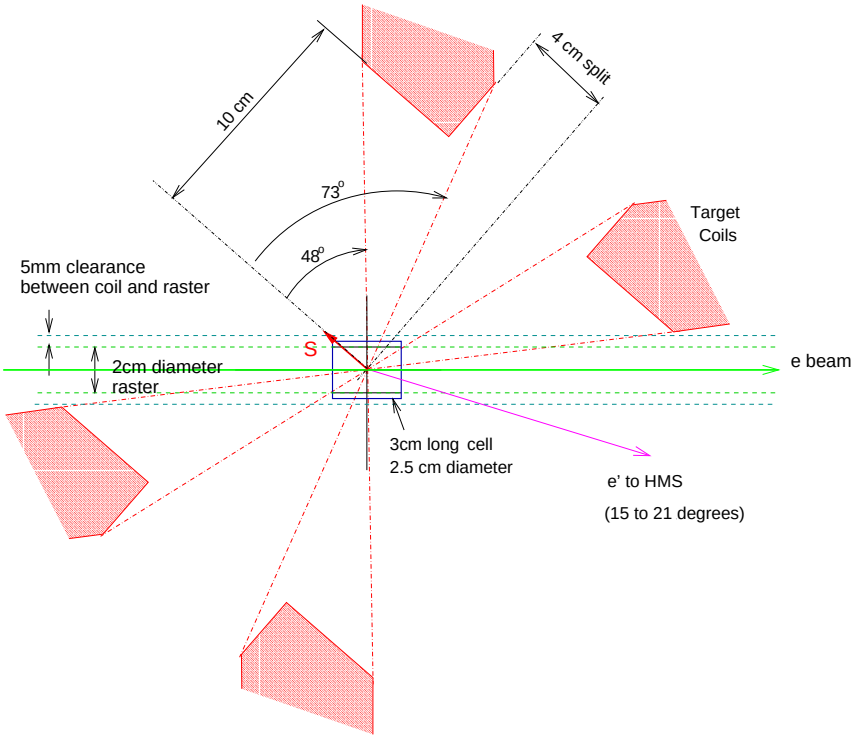

Figure 8: The 3 cm long by 1 inch diameter cylindrical target cell with the single loop coil used for measuring the proton polarization. Drawing not to scale.

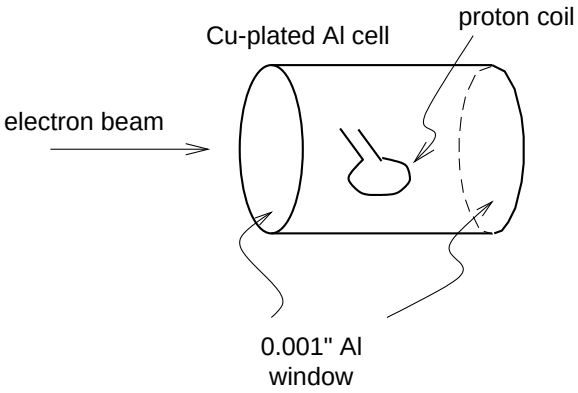

experiment. During previous experiments the field direction has been measured to 0.1° and we require the same precision.

3.4 Spectrometer

For the proposed experiment, only scattered electrons will be detected. Elastic events are identified by the scattering angle and momentum of electrons. Good resolutions in both the angle and momentum will help to reduce the elastic peak width and the quasi-elastic background. We will use the High Momentum Spectrometer (HMS) for detecting electrons. A gas cherenkov detector which is part of the standard equipment) is needed in HMS for rejecting pions. The central momentum of HMS can be calculated from the dipole field magnitude to 1×10^{-3} level [24]. The central angle can be determined to 0.3 mrad (?). In Section 4.4 we will give the simulation results of both elastic and quasi-elastic events and estimate the dilution factor.

3.5 Acceptance Effect due to Target Magnetic Field

Due to the strong magnetic field the scattered electrons will be bended up by $\approx 5^\circ$. This will cause a tilt of the scattering plane. The direct effects are that there is a correction to the target spin polar angle $\theta^\star$ and $\phi^\star \neq 0$. Figure 9 shows HMS acceptance for electrons at $Q^2 = 2.10$ (GeV/c)^2. Overall, for measurements at $Q^2 = 2.10$ and $Q^2 = 3.50$ (GeV/c)^2 the bending is small and the scattering angle is close to the HMS central setting. The change in the counting rate is negligible.

Figure 9: HMS acceptance for $E' = 4.881$ electrons with (red) and without (black) target field. With target field electrons with initial $\phi_{targ} < 0$ (vertical up) will reach the center of HMS.

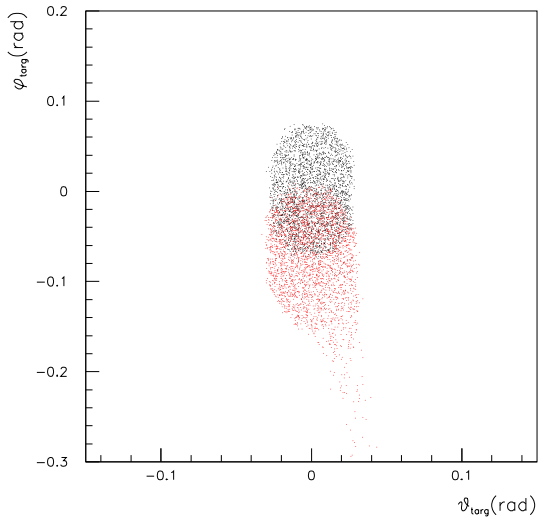

3.6 Low Q^2 Measurement

We will measure elastic asymmetry at $Q^2 = 0.19$ (GeV/c)^2 to 2% level to check the product of target and beam polarizations. The beam energy will be changed to one pass and the HMS angle is 21.65°. The target field needs to be rotated to 21.65° to the right of beam-line in order to avoid the large bending of scattered low momentum electrons. Rotating the target field will take about one day. Since the magnet coils (thus the field axis) are well surveyed relative to the scattering chamber, it is enough to have only one field axis measurement during the experiment.

3.7 Data Analysis

The physics asymmetries can be extracted from the raw asymmetries as

$$A_{\parallel,\perp} = \frac{A_{raw}(1-\eta_{A_{\rm N}})}{P_{beam}P_{targ}f} \tag{1}$$

where $P_{beam} = 80\%$ and $P_{targ} = 75\%$ are beam and target polarization, f is the target dilution factor and $\eta_{A_{\rm N}}$ is a correction factor due to the asymmetry of nitrogen in $^{15}{\rm NH}_3$ (see Section 4.5). Ratio G_E^p/G_M^p is extracted using Eq. (16) and its uncertainty from Eq. (17).

The error in asymmetry A is

$$\Delta A = \Big\{\Big(\frac{\Delta A_{raw}}{f P_b P_t}\Big)^2 + A^2\Big[(\frac{\Delta P_b}{P_b})^2 + (\frac{\Delta P_t}{P_t})^2 + (\frac{\Delta f}{f})^2\Big]\Big\}^{1/2}, \tag{2}$$

$$\text{with} \qquad \Delta A_{raw} = \frac{1}{\sqrt{N}} \tag{3}$$

Here N is total number of events. From Eq. (16) one can extract G_E^p/G_M^p from asymmetries and its uncertainty is calculated using Eq. (17). Detailed formula for error propagation are given in Appendix A and B.

4 Expected Uncertainties and Rate Estimation

In this section we first list all uncertainty sources. Then we calculate the rate, expected total uncertainties on $\mu G_E^p/G_M^p$ and beam time.

4.1 Experimental Systematics

We estimate the uncertainty in the beam polarization to be 1.5% and the target polarization has 2.5% uncertainty. Other error sources include those from the target spin angle, beam energy $\Delta E/E = 2\times10^{-4}$, HMS central momentum $\Delta E'/E' = 1\times10^{-3}$ [24], and central angle $\Delta\theta = 0.3$ mrad. Formula for error propagation from these experimental systematics to $\mu G_E^p/G_M^p$ are given in Appendix B. The largest systematic uncertainty comes from target polarization. At $\Delta P_{targ}/P_{targ} = 2.5\%$ the uncertainty in $\mu G_E^p/G_M^p$ is about $2/3$ of the statistical uncertainty.

4.2 Beam Charge Measurement

The beam current can be measured to 5% level at 100 nA. The effect on the measured asymmetries is negligible.

4.3 Target Polarization

Target polarization can be measured to 2.5% using NMR.

4.4 Target Dilution Factor

The dilution factor is due to the quasi-elastic events from nitrogen in NH_3 and from other material listed in Table 1. Since the reconstructed elastic peak at forward angles typically has < 20 MeV FWHM, while quasi-elastic events are smeared by Fermi motion at $p_F/M = \pm 10\%$ level if Fermi momentum $p_F \approx 200$ MeV/c, about 80% of quasi-elastic events will be excluded using a cut in $\delta E' \equiv E' - E'_{el}$ where E'_{el} is the electron energy measured by HMS and E'_{el} is the energy of elastically scattered electrons calculated from the scattering angle θ. Figure 10 shows the simulated elastic events (red), quasi-elastic events (green) and the sum (blue) for 1 mC beam charge.

The dilution factor is defined as

$$f = \frac{N_p}{N_p + N_{\rm QE}} \tag{4}$$

where N_p and $N_{\rm QE}$ are yield of $e-p$ elastic events and quasi-elastic from ^{15}N and other target material. Since the actual angular resolution of the HMS is usually not as good as the COSY model used in the simulation, we use $f = 0.5$ as a conservative estimation for all three kinematics in the rate and uncertainty estimation. This value is also consistent with previous experiment [27].

We will take data on a nitrogen cell with approximately the same geometry as NH_3 cell to measure quasi-elastic cross section from nitrogen and all other target material. The dilution factor was determined to $2.5 \sim 3\%$ during previous experiment [27]. We use 2.5% in the uncertainty estimation.

4.5 Nitrogen Asymmetry

The nitrogen in NH_3 is polarized and will contribute to the asymmetry. In the shell model, ^{15}N nuclei has one unpaired proton which can be polarized. The polarization of the unpaired proton in ^{15}N is reduced from that of a free proton by several factors. First, the nitrogen in ^{15}N is polarized up to only $1/6$ of the proton, based on the Equal Spin Temperature (EST) hypothesis. Experimental data show even lower polarization, as shown in Fig. 11. Secondly, the proton in a polarized ^{15}N is only polarized to a certain amount. This quantity, called the effective nucleon polarization, has been estimated in two ways. In a model independent method [30, 31], $P_{p/^{15}\rm N} \approx -0.22$ based on isospin symmetry and data from beta decay of the mirror nuclei

Figure 10: Expected spectra on $\delta E' \equiv E' - E'_{el}$ for the proposed measurements at $Q^2 = 0.19$ (top), 2.10 (middle) and 3.50 (GeV/c)^2 (bottom). Simulations were performed using SIMC without HMS collimators, ^{15}N and ^{4}He quasi-elastic events were simulated by ^{12}C spectral functions and all other material were using ^{56}Fe spectral function. The blue shows the sum of elastic and quasi-elastic events. Black lines show cut in $\delta E'$ used to obtain elastic rate and dilution f.

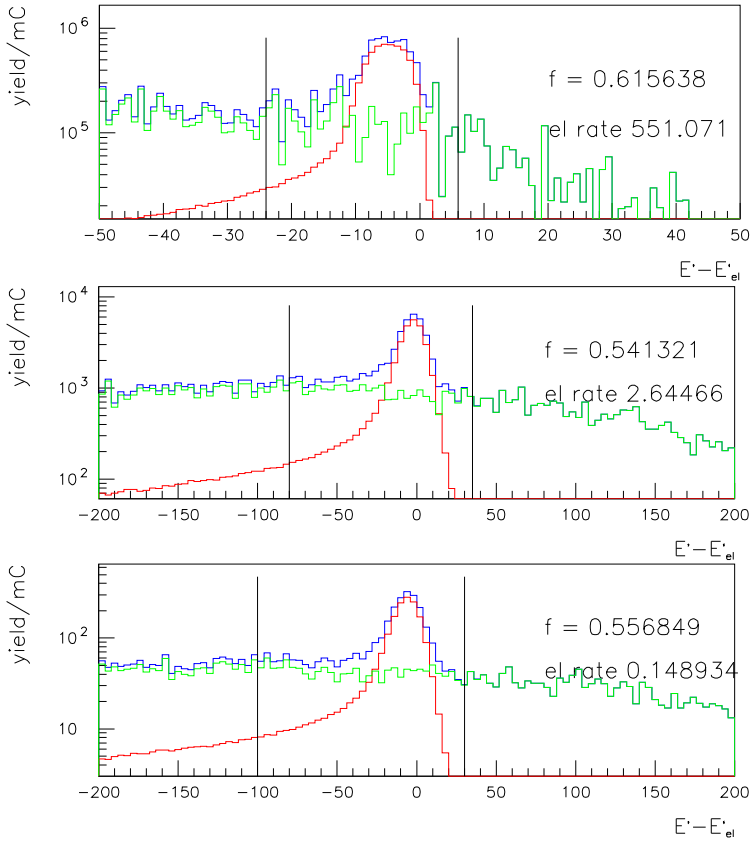

^{15}O. In the shell model, the proton in ^{15}N is aligned anti-parallel to the nuclear spin $1/3$ of the time, hence $P_{p/^{15}\mathrm{N}} = -0.33$. Overall, the polarization of the unpaired proton is at most $(0.22 \sim 0.33) \times 1/6 P_p = 0.037 \sim 0.055 P_p$ and if we take the measured data, is about $(0.22 \sim 0.33) \times 1/10 P_p = (0.022 \sim 0.033) P_p$. In addition, only about $1/15$ of ^{15}N quasi-elastic events are from the $p_{1/2}$ proton and ^{15}N contribute $> 95\%$ of all quasi-elastic events. Hence the correction to the measured asymmetry A_m due to nitrogen is

$$A_m = f A_p + \frac{0.95(1-f)}{15} A_{p/^{15}\mathrm{N}} = f A_p \Big(1 + (0.014 \sim 0.021)\frac{1-f}{f}\Big) \quad (5)$$

$$A_p = \frac{A_m}{f}\Big(1 - (0.0175 \pm 0.0035)\Big) \quad \text{if } f = 0.5 \quad (6)$$

Figure 11: Polarization of nitrogen P_N in $^{15}NH_3$ *vs.* proton polarization P_p measured during E155 [29]. The black circle is the prediction in Equal Spin Temperature (EST) hypothesis and the red dots is what were actually measured.

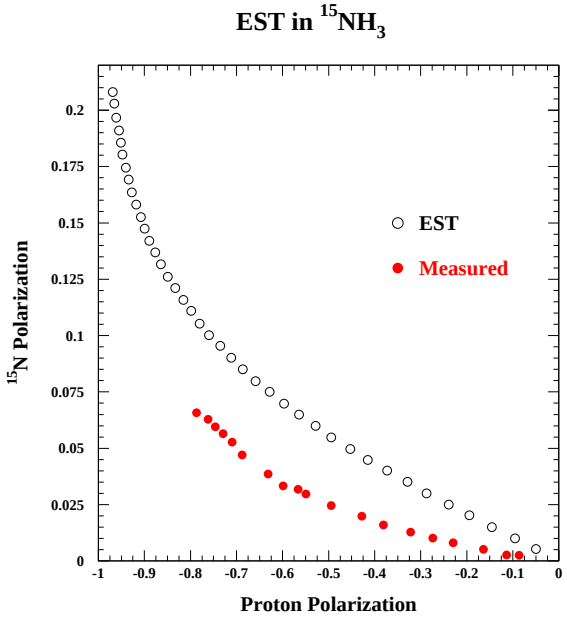

Compared to the usually used $A = \frac{A_m}{f}$, we need to apply 1.75% correction with $\pm 0.35\%$ uncertainty for all three Q^2 points.

4.6 Background

For our measurement the main background comes from the quasi-elastic scattering from nitrogen and materials on the beam path. This part is stated in the last section. The π^- background is expected to be small and will be rejected by the gas cherenkov detector so the effect on the measured asymmetry is negligible.

4.7 Electromagnetic Radiative Corrections

The EM radiative corrections were simulated using Mo&Tsai. The uncertainty in the radiative corrections on the asymmetries is negligible.

4.8 Deadtime Correction

The rate of our proposed measurement is very low, $\sim$Hz, hence the electronic dead time correction is small and the effect on the measured asymmetry is negligible. Computer deadtime can be

measured by triggers and the uncertainty is determined by the statistics of each run. We require a run to have at least 1M events hence the uncertainty in the measured deadtime is 0.1%.

4.9 Optimization of Kinematics

We optimize the kinematics based on the following conditions:

- For a given Q^2, the rate is maximized by varying beam energy and scattering angle;
- For given Q^2 and beam energy, the total uncertainty of G_E^p/G_M^p is minimized by varing target spin angle;
- Target coils do not interfere with either beam-line or scattered electrons. A 0.5 cm clearance is required between the edge of coils and particle trajectory.

Results are shown in Fig. 12 and 13. We choose to use 6 GeV beam. Target spin will be pointing to the left and aligned at 139° *w.r.t* beam-line.

Figure 12: Expected total uncertainties of $\mu G_E^p/G_M^p$ *vs.* target spin angle for $E_b = 6$ (GeV) and fixed beam time, 32.0 and 262.1 hours for $Q^2 = 2.10$ and 3.50 (GeV/c)^2, respectively. Here negative spin angle means the target spin is pointing to the left of beam-line. Red (blue) boxes show the interference between coils and beam-line (scattered electrons). Red stars shows the selected kinematics.

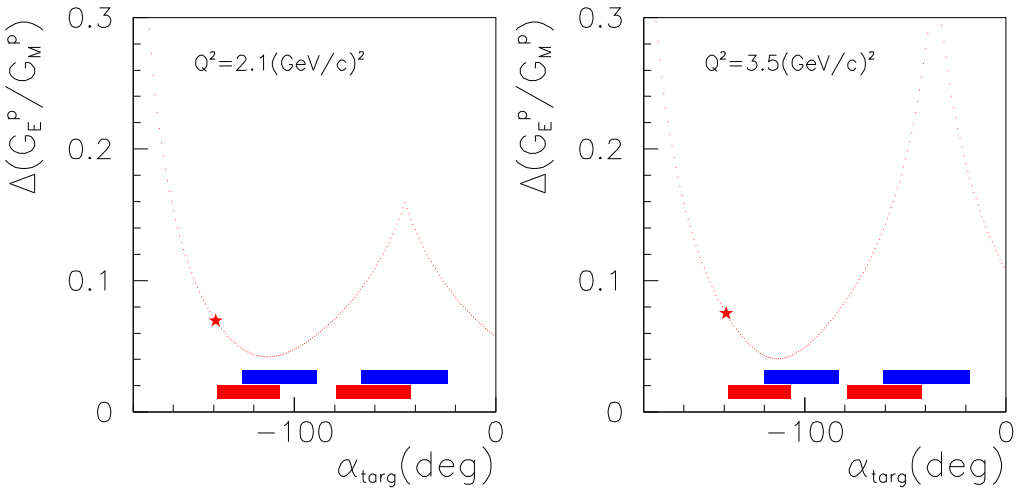

Figure 13: Expected total uncertainties of $\mu G_E^p/G_M^p$ *vs.* beam energy for fixed beam time, 32.0 and 262.1 hours for $Q^2 = 2.10$ and 3.50 (GeV/c)^2, respectively. Hence we choose to use 6 GeV beam.

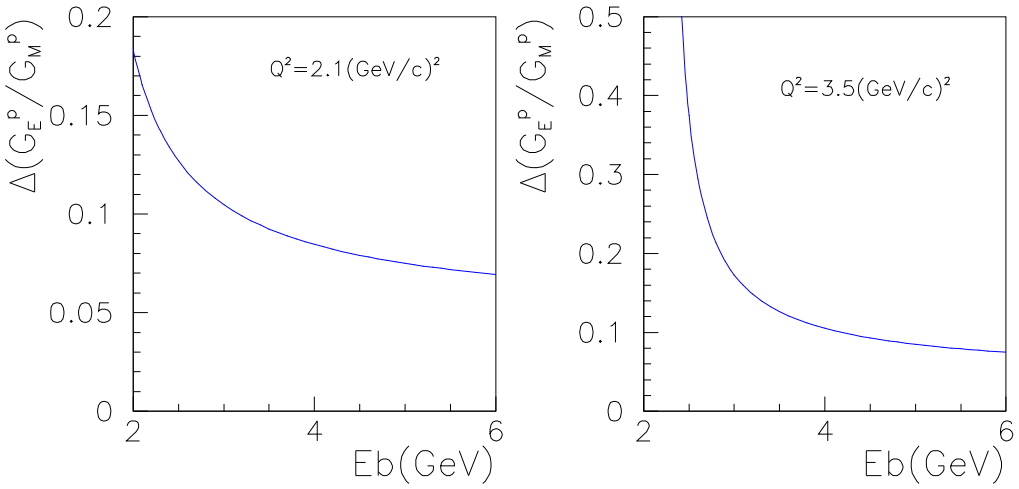

4.10 Summary of Rate and Expected Uncertainties

We use Bosted fit for G_M^p and the G_E^p/G_M^p value from polarization transfer data [13] to calculate the elastic $e-p$ cross section. Using 3 cm target cell and 85 nA the luminosity available is 8.5×10^{34} cm^2/s. Kinematics, rates and expected uncertainties for the proposed measurements are given in Table 2. The expected results are shown in Fig. 14.

Figure 14: Expected results and full uncertainties of the proposed measurements (red solid circles) along with world data. Curves are the same as in Fig. 2.

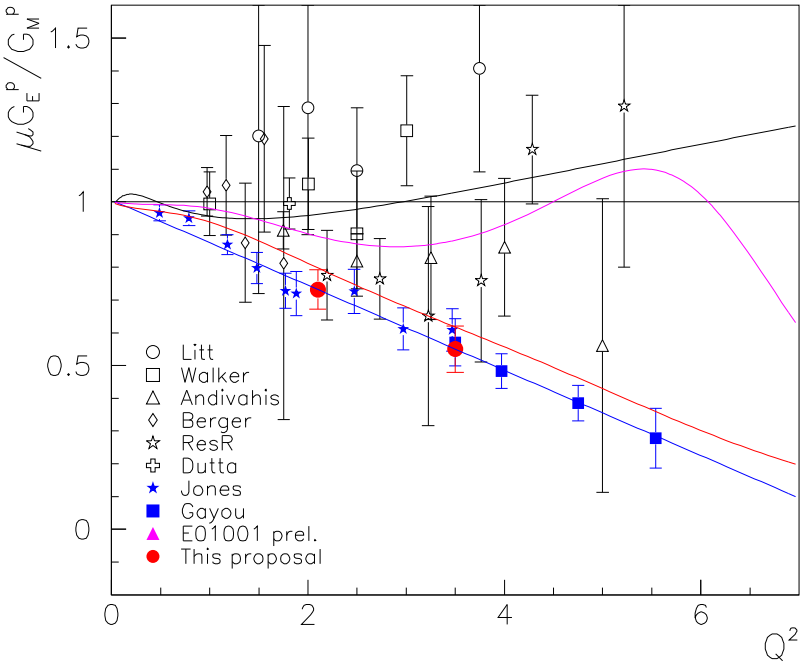

Table 2: Kinematics, rate and expected uncertainties for the proposed measurements.

Q^2 (GeV/c)^2	0.19	2.10	3.50
E_b (GeV)	1.20	6.00	6.00
θ_e	21.65°	15.39°	21.65°
E' (GeV)	1.101	4.881	4.135
θ_p	66.46°	45.03°	35.27°
p_p (GeV/c)	0.443	1.831	2.642
$\theta^\star$	88.10°	93.99°	103.78°
$\phi^\star$	0.00°	176.75°	176.88°
A_{el}	-0.198	0.119	0.200
($A_{el,bosted}$)	-0.201	0.140	0.255
A_{raw}	-0.0595	0.0357	0.0599
σ (nb/sr)	2308.683	5.893	0.332
elastic rate (SIMC, Hz)	494.520	2.554	0.144
total rate (el rate/f, Hz)	989.040	5.109	0.288
N_{tot}	1414K	1176K	543K
Uncertainty on asymmetries			
Statistical	2.000%	3.654%	3.203%
Uncertainty on $\mu G_E^p/G_M^p$			
$\Delta P_{beam}/P_{beam} = 1.5\%$	-	0.0174	0.0222
$\Delta P_{targ}/P_{targ} = 2.5\%$	-	0.0290	0.0370
Target dilution $\Delta f/f = 2.5\%$	-	0.0290	0.0370
Nitrogen asymmetry	-	0.0041	0.0052
Deadtime correction	-	0.0012	0.0015
$\Delta p_p/p_p = 5 \times 10^{-4}$	-	0.0001	0.0001
$\Delta\theta_e = 0.3$ mrad	-	0.0008	0.0005
Target spin orientation (inp) 0.1°	-	0.0002	0.0001
Target spin orientation (oop) 0.1°	-	0.0098	0.0069
Total syst.	-	0.0458	0.0576
Total stat.	-	0.0424	0.0474
Beam time (hours)	0.2	32.0	262.1
Expected $\mu G_E^p/G_M^p$ and total uncertainty	-	0.732 ± 0.060	0.550 ± 0.071

$\diamond$ E_b is beam energy;
$\diamond$ θ_e and E' are the energy and momentum of scattered electrons (HMS);
$\diamond$ θ_p and p_p are the energy and momentum of scattered protons (not detected);
$\diamond$ $\theta^\star$ and $\phi^\star$ are the polar and azimuthal angles of target spin;
$\diamond$ A_{el} and $A_{el,bosted}$ are elastic asymmetries calculated from Hall A polarization transfer (PT) fit and Bosted fit, respectively;
$\diamond$ A_{raw} is expected measured asymmetry using PT fit;
$\diamond$ N is total number of events;

5 Beam Time Request

Our beam time request is given in Table 3. We ask for 14 days total beam time, including production data taking, target dilution factor measurement and Møller measurement. We ask for 4 days overhead time for beam energy change and measurement of the target field direction. Time needed for target installation is not given here.

Table 3: Beam time request (in hours) and spectrometer setting for the proposed measurements.

Q^2 (GeV/c)^2	0.19	2.10	3.50
E_b (GeV)	1.20	6.00	6.00
θ_{HMS}	21.65°	15.39°	21.65°
p_{HMS} (GeV/c)	1.101	4.881	4.135
Production time	0.2	32.0	262.1
nitrogen run	6	6	6
Møller measurement	6	6	
arc measurement	4	4	
Total beam time	334		
Pass change	12		
Target anneal	37		
Target field rotation	24		
Target field survey	12		
Spectrometer angle survey	4×2		
Total overhead	93		

6 Summary

We propose to make measurements of G_E^p/G_M^p via the polarization asymmetry in doubly polarized elastic $\vec{p}(\vec{e},e')p$ scattering at $Q^2 = 2.10$ and 3.50 (GeV/c)^2. Assuming 80% beam polarization and 85 nA current, we request 14 days of total beam time and four days overhead. The proposed measurement will provide the first data for $\mu G_E^p/G_M^p$ from the $\vec{p}(\vec{e},e')p$ asymmetry method in intermediate Q^2 range to a good precision. This new method is less sensitive to possible two-photon exchange contributions than the Rosenbluth separation, and it does not suffer from possible systematic uncertainties due to spin precession which exist in previous polarization transfer data. These data will provide an important check on the polarization transfer results. When combined with the recent check on the Rosenbluth sparation results, these new data will either confirm that two-photon (and perhaps higher order) exchange is a necessary ingredient in future calculations, or they will point to a systematic error in prior experimental techniques.

Acknowledgment

A Doubly Polarized Elastic Scattering

For elastic scattering the unpolarized cross section is given by

$$\Big(\frac{\mathrm{d}\sigma}{\mathrm{d}\Omega \mathrm{d}E'}\Big)^u \;=\; \sigma_M \frac{E'}{E}\Big(\frac{G_E^2+\tau G_M^2}{1+\tau} + 2\tau G_M^2 \tan^2(\theta/2)\Big)\,, \tag{7}$$

where $Q^2 = 4EE'\sin^2(\theta/2)$, $\tau = Q^2/(4M^2)$, the energy of scattered electrons is $E' = E/[1+\frac{2E}{M}\sin^2(\theta/2)]$, M is the nucleon mass, E is the beam energy and θ is the electron scattering angle. The Mott cross section is

$$\sigma_M \equiv \Big(\frac{\mathrm{d}^2\sigma}{\mathrm{d}\Omega}\Big)_{Mott} \;=\; \frac{\alpha^2\cos^2\frac{\theta}{2}}{4E^2\sin^4\frac{\theta}{2}}\,. \tag{8}$$

The momentum and the angle of the scattered protons are

$$p_p \;=\; \sqrt{Q^2+(\frac{Q^2}{2M})^2}\ \text{and} \tag{9}$$

$$\cos\theta_p \;=\; \frac{(M+E)\sqrt{M^2+p_p^2}-M^2-ME}{p_pE}\,. \tag{10}$$

For the case of polarized electrons scattering off a polarized nucleon target, the cross section difference between opposite electron helicity states is given by [23]

$$\frac{1}{2}[\sigma^+ - \sigma^-] \;=\; -2\sigma_M\frac{E'}{E}\sqrt{\frac{\tau}{1+\tau}}\tan\frac{\theta}{2}\Bigg\{\sqrt{\tau(1+(1+\tau)\tan^2\frac{\theta}{2})}\cos\theta^\star G_M^2 + \sin\theta^\star\cos\phi^\star G_M G_E\Bigg\}\,, \tag{11}$$

where the superscript $\pm$ denotes the helicity of the incident electrons, θ^* and ϕ^* are the polar and the azimuthal angles of the target spin direction as shown in Fig. 15. The asymmetry is

$$\begin{aligned} A \;&\equiv\; \frac{\sigma^+-\sigma^-}{\sigma^++\sigma^-} \\ &=\; -\frac{2\sqrt{\frac{\tau}{1+\tau}}\tan\frac{\theta}{2}\Big\{\sqrt{\tau(1+(1+\tau)\tan^2\frac{\theta}{2})}\cos\theta^\star G_M^2 + \sin\theta^\star\cos\phi^\star G_M G_E\Big\}}{\frac{G_E^2+\tau G_M^2}{1+\tau}+2\tau G_M^2\tan^2(\theta/2)}\,, \end{aligned} \tag{12}$$

Equation (12) can be written as

$$(\frac{G_E}{G_M})^2 + B(\frac{G_E}{G_M}) + C \;=\; 0\,, \tag{13}$$

Figure 15: Polar and azimuthal angles of the target spin. Here $\vec{S}$ is the target spin, $\vec{q}$ is the three momentum transfer. The $z^\star$ axis is defined by $\vec{q}$, $y^\star$ axis is defined by $\vec{k} \times \vec{k}'$ with $k(k')$ the three momentum of the incident and scattered electrons.

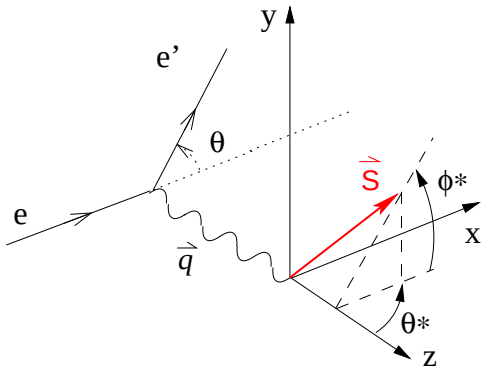

where

$$B = \frac{2}{A}\sqrt{\tau(1+\tau)}\tan\frac{\theta}{2}\sin\theta^\star\cos\phi^\star\,, \tag{14}$$

$$C = \tau + 2\tau(1+\tau)\tan^2\frac{\theta}{2} + \frac{2\cos\theta^\star}{A}\left\{\sqrt{\tau(1+\tau)}\tan\frac{\theta}{2}\sqrt{\tau\left[1+(1+\tau)\tan^2\frac{\theta}{2}\right]}\right\} \tag{15}$$

with A the measured elastic asymmetry. Therefore ratio G_E/G_M can be calculated as

$$\frac{G_E}{G_M} = \frac{1}{2}(-B \pm \sqrt{B^2-4C})\,, \tag{16}$$

the sign is kinematic dependent. The uncertainty due to the error in asymmetry is given by

$$\Delta(\frac{G_E}{G_M}) = \frac{\Delta A}{2}\left|\left(\frac{\mathrm{d}B}{\mathrm{d}A}\right)\left(-1 \pm \frac{B}{\sqrt{B^2-4C}}\right) \pm \left(\frac{\mathrm{d}C}{\mathrm{d}A}\right)\frac{-2}{\sqrt{B^2-4C}}\right| \tag{17}$$

$$\text{where} \quad \frac{\mathrm{d}B}{\mathrm{d}A} = -\frac{B}{A}$$

$$\text{and} \quad \frac{\mathrm{d}C}{\mathrm{d}A} = -\frac{C-[\tau+2\tau(1+\tau)\tan^2\frac{\theta}{2}]}{A}$$

B Error Propogation of Systematic Uncertainties for G_E^p/G_M^p

The uncertainty in G_E^p/G_M^p due to the uncertainty in asymmetry ΔA is given by Eq. (17) where ΔA is from Eq. (2). In this appendix we give experimental systematics due to uncertainties in E_b, E', θ, $\theta^\star$ and $\phi^\star$.

From Eq. (16) the uncertainty in G_E/G_M due to the uncertainty in E_b is given by

$$\Delta(\frac{G_E}{G_M}) \;=\; \frac{\Delta E_b}{2}\Big|\Big(\frac{\mathrm{d}B}{\mathrm{d}E_b}\Big)\Big(-1 \pm \frac{B}{\sqrt{B^2-4C}}\Big) \pm \Big(\frac{\mathrm{d}C}{\mathrm{d}E_b}\Big)\frac{-2}{\sqrt{B^2-4C}}\Big| \tag{18}$$

the same equation stands for E', θ, $\theta^\star$ and $\phi^\star$. For E_b we have

$$\frac{\mathrm{d}B}{\mathrm{d}E_b} \;=\; \frac{\partial B}{\partial \tau}\frac{\mathrm{d}\tau}{\mathrm{d}E_b}\,, \quad \frac{\mathrm{d}C}{\mathrm{d}E_b} = \frac{\partial C}{\partial \tau}\frac{\mathrm{d}\tau}{\mathrm{d}E_b} \tag{19}$$

where

$$\begin{aligned}
\frac{\partial B}{\partial \tau} &= \frac{1}{2}(\frac{B}{\tau} + \frac{B}{1+\tau})\,, \\
\frac{\partial C}{\partial \tau} &= 1 + 2(1+\tau)\tan^2\frac{\theta}{2} + \frac{\tan\frac{\theta}{2}}{2A}\cos\theta^\star\Bigg\{2\sqrt{(1+\tau)\Big[1+(1+\tau)\tan^2\frac{\theta}{2}\Big]} \\
&\quad + \sqrt{\frac{1+(1+\tau)\tan^2\frac{\theta}{2}}{1+\tau}} + \tau\tan\frac{\theta}{2}\sqrt{\frac{1+\tau}{1+(1+\tau)\tan^2\frac{\theta}{2}}}\Bigg\} \\
\text{and } \frac{\mathrm{d}\tau}{\mathrm{d}E_b} &= \frac{\tau}{E_b}\,,
\end{aligned} \tag{20}$$

For θ we have

$$\frac{\mathrm{d}B}{\mathrm{d}\theta} \;=\; \frac{\mathrm{d}B}{\mathrm{d}\theta} + \frac{\partial B}{\partial \tau}\frac{\mathrm{d}\tau}{\mathrm{d}\theta}\,, \quad \frac{\mathrm{d}C}{\mathrm{d}\theta} = \frac{\mathrm{d}C}{\mathrm{d}\theta} + \frac{\partial C}{\partial \tau}\frac{\mathrm{d}\tau}{\mathrm{d}\theta} \tag{21}$$

where

$$\frac{\mathrm{d}\tau}{\mathrm{d}\theta} \;=\; \frac{E_b E'}{2M^2}\sin\theta\,, \quad \frac{\mathrm{d}B}{\mathrm{d}\theta} = \frac{B}{\sin\theta}$$

For E' we have

$$\frac{\mathrm{d}B}{\mathrm{d}E'} \;=\; \frac{\partial B}{\partial \tau}\frac{\mathrm{d}\tau}{\mathrm{d}E'} + \frac{\mathrm{d}B}{\mathrm{d}\theta^\star}\frac{\mathrm{d}\theta^\star}{\mathrm{d}E'}\,, \quad \frac{\mathrm{d}C}{\mathrm{d}E'} = \frac{\partial C}{\partial \tau}\frac{\mathrm{d}\tau}{\mathrm{d}E'} + \frac{\mathrm{d}C}{\mathrm{d}\theta^\star}\frac{\mathrm{d}\theta^\star}{\mathrm{d}E'} \tag{22}$$

$$\text{where } \frac{\mathrm{d}\tau}{\mathrm{d}E'} \;=\; \frac{\tau}{E'}\,.$$

The target spin polar angle $\theta^\star$ is determined by the field orientation and the proton scattering angle. The target field direction can be measured to 0.1° and the uncertainty in the proton angle is determined by the electron momentum $\Delta E'/E'$ as

$$\frac{\mathrm{d}\theta^\star}{\mathrm{d}E'} \;=\; \frac{\mathrm{d}\theta_p}{\mathrm{d}E'} = \frac{(M+E)M}{(2M+\nu)^{3/2}E\sin\theta_p}\,. \tag{23}$$

References

[1] E.L. Lomon, *Phys. Rev. C* **64**, 035204 (2001).

[2] S.J. Brodsky and G. Farrar, *Phys. Rev. D* **11**, 1309 (1975).

[3] S.J. Brodsky and G.P. Lepage, *Phys. Rev. D* **22**, 2157 (1981).

[4] P.L. Chung and F. Coester, *Phys. Rev. D* **44**, 229 (1991).

[5] M.R. Frank, B.K. Jennings and G.A. Miller, *Phys. Rev. C* **54**, 920 (1996).

[6] R.F. Wagenbrunn *et al.*, *Phys. Lett. B* **511**, 33 (2001); S. Boffi *et al. Eur. Phys. J. A* **14**, 17 (2002), or e-Print hep-ph/0108271

[7] F. Cardarelli and S. Simula, *Phys. Rev. C* **62**, 065201 (2000); S. Simula, e-Print nucl-th/0105024.

[8] D.H. Lu, A.W. Thomas and A.G. Williams, *Phys. Rev. C* **57**, 2628 (1998).

[9] G.Holzwarth, *Zeitschr. Fuer Physik A* **356**, 339 (1996), e-Print hep-ph/9606336; e-Print hep-ph/0201138 and ref. therein.

[10] A. Afanasev, *priv. comm.*

[11] A.F. Sill *et al.*, *Phys. Rev. D* **48**, 29 (1993).

[12] M. K. Jones *et al.*, *Phys. Rev. Lett.* **84**, 1398 (2000), e-Print: nucl-ex/9910005;

[13] O. Gayou *et al.*, *Phys. Rev. Lett.*, **88**, 092301 (2002), e-Print: nucl-ex/0111010.

[14] O. Gayou *et al.*, *Phys. Rev. C* **64**, 038202 (2003).

[15] J. Arrington, *Eur. Phys. J.* **A17**, 311 (2003), e-Print Archive: hep-ph/0209243; *Phys. Rev.C* **68**, 034325 (2003), e-Print Archive: nucl-ex/0305009;

[16] P. Bosted, *Phys. Rev. C* **51**, 409 (1995).

[17] H. Budd, A. Bodek and J. Arrington, *to be published in Nucl. Phys. B*, e-Print Archive: hep-ex/0308005.

[18] J. Arrington and R. Segel, JLab E01-001, New Measurement of (GE/GM) for the Proton.

[19] E. Brash, C. Perdrisat and V. Punjabi, JLab E01-109, Measurement of Gep/Gmp to Q2=9 GeV2 via Recoil Polarization.

[20] P.A.M. Guichon and M. Vanderhaeghen, e-Print: hep-ph/0306007.

[21] P.G. Blunden, W. Melnitchouk and J.A. Tjon, e-Print:nucl-th/0306076.

[22] M.P. Rekalo and E. Tomasi-Gustafsson, e-Print:nucl-th/0307066.

[23] T.W. Donnelly and A.S. Raskin, Annals of Phys., 169, 247 (1986).

[24] Here should go a Hall C NIM paper;

[25] H.-G. Zhu, *Ph.D. thesis*, Univ. of Virginia, Charlottesville, VA (2000).

[26] D. Day, JLab E93-026, The Charge Form Factor of the Neutron.

[27] O. Rondon-Aramayo, JLab E01-006, Precision Measurement of the Nucleon Spin Structure Functions in the Region of the Nucleon Resonances.

[28] P.E. Raines, *Ph.D. thesis*, Univ. of Pennsylvania, (1996).

[29] H.-G. Zhu, *priv. comm.*

[30] K. Sugimoto, *Phys. Rev.* **182**, 1051 (1969).

[31] O.A. Rondon, *Corrections to nucleon spin structure asymmetries measured on nuclear polarized targets*, unpublished.